SAND2000-0806J

Gravity-driven Dense Granular Flows

Deniz Ertaş[1*], Gary S. Grest[2], Thomas C. Halsey[1], Dov Levine[3], and Leo Silbert[2]
[1] *Corporate Strategic Research, ExxonMobil Research and Engineering, Route 22 East, Annandale, New Jersey 08801*
[2] *Sandia National Laboratories, Albuquerque, New Mexico 87185-1411*
[3] *Department of Physics, Technion, Haifa, 32000 Israel*
(March 14, 2000)

We report and analyze the results of numerical studies of dense granular flows in two and three dimensions, using both linear damped springs and Hertzian force laws between particles. Chute flow generically produces a constant density profile that satisfies scaling relations suggestive of a Bagnold grain inertia regime. The type of force law has little impact on the behavior of the system. Failure is *not* initiated at the surface, consistent with the absence of surface flows and different principal stress directions at vs. below the surface.

46.55.+d, 45.70.Cc, 46.25.-y

Understanding the behavior of granular materials has been a great challenge to scientists [1,2] and engineers [3,4]. One major hurdle has been the lack of a formal connection between the complex but relatively well-understood world of contact mechanics [5], which describes the nature and dynamics of intergranular interactions, and empirical continuum models that describe the macroscopic behavior of the system. It is our ultimate goal to construct continuum theories that are derived from contact mechanics without further assumptions, even though their very existence has been questioned [6]. Given the extreme difficulty of studying all but the simplest geometries analytically, we perform simulations of granular dynamics in order to directly observe the consequences of contact mechanics at the macroscopic level. We observe several remarkable features in gravity-driven dense granular flows down an inclined plane, denoted henceforth as "chute flow":

(1) At steady-state, the packing fraction ϕ remains constant as a function of depth, beyond a dilatant surface region a few layers thick (Fig. 1.) The compacting influence of increasing stress due to the weight of grains overhead is balanced by increasing velocity fluctuations towards the bottom of the pile.

(2) Unlike Couette flows, the entire pile is in motion and surface-only flows are not observed. Failure is initiated at the bottom wall, not at the surface.

(3) Components of the stress tensor and the square of the strain rate grow linearly with depth, indicative of Bagnold grain-inertia behavior [7].

(4) Normal stresses differ from each other [8] in subtle yet systematic ways (Fig. 2), which we do not fully understand.

We report results of large scale molecular dynamics simulations of chute flow in two and three dimensions (2D and 3D), with interparticle interactions betweeen the (monodisperse) spheres modeled using both damped linear springs and Hertzian contact forces, with static friction. Detailed results of the simulations will be presented elsewhere [9]. The main obstacle for experiments and simulations so far had been the difficulty of reaching and maintaining steady state. Previous simulations [10–12] employed very few particles or did not reach steady state [13]. All of these simulations were in 2D with the exception of Ref. [10]. Experiments on chute flow [14,15] did not involve deep piles. Different effects of flow were also studied in simulation, such as size segregation [16].

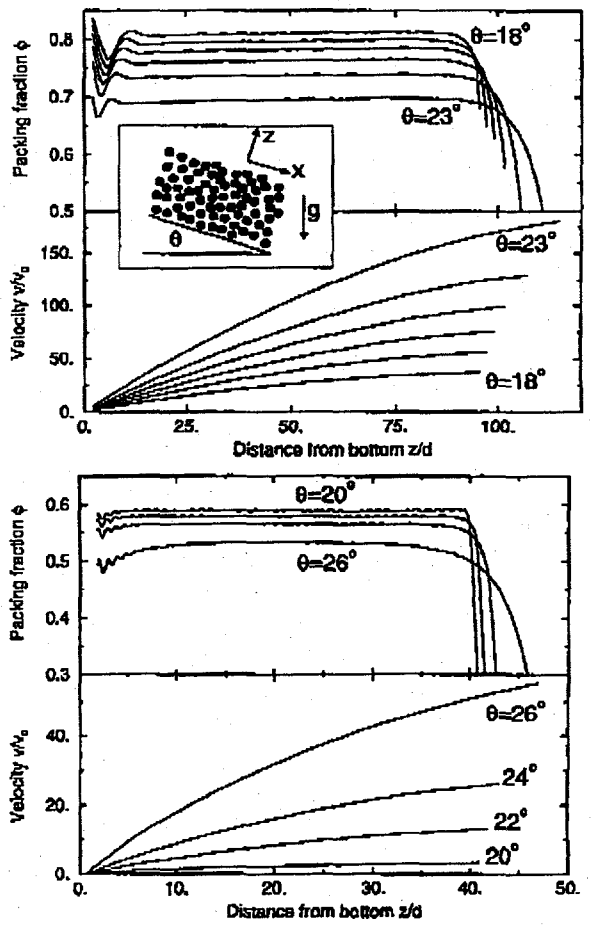

FIG. 1. Density and velocity profiles as a function of height from the bottom of the piles for 2D (top) and 3D (bottom) simulations. Inset shows a schematic of the geometry. Results are for 10 000 particles in 2D and 8 000 in 3D.

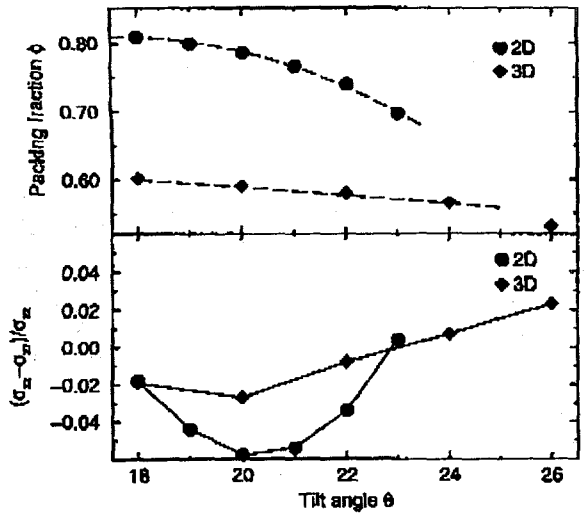

FIG. 2. Tilt dependence of the packing fraction (top) and the normal stress anomaly $(\sigma_{zz} - \sigma_{xx})/\sigma_{zz}$ (bottom) in the region of constant packing fraction. The dashed lines are fits to the forms Eq. (8 -9).

The 3D simulation boxes contain spheres of diameter d and mass m, supported by a fixed bottom on the $x-y$ plane. The bottom wall is constructed from a cross-section of a random close packing of identical spheres, providing a rough surface. Periodic boundary conditions are imposed along x and y directions. 2D simulations follow the same procedure, except that particles are restricted to the $x-z$ plane and the bottom consists of a regular array of particles of diameter $2d$. In both cases, there is no slip at the bottom, unlike 2D simulations with a regular array of particles of diameter d, where some slip is observed. Tilting is accomplished by rotating the gravity vector $\mathbf{g}$ in the $x-z$ plane by the tilt angle θ away from the $(-\hat{z})$ direction. This ensures that the free surface is always normal to the $\hat{z}$ axis. In 3D, most of our results are for 8 000 particle systems with a simulation cell of size $L_x = 18.6d$ and $L_y = 9.3d$, resulting in a pile roughly 40 particles deep near θ_r. In 2D, $L_x = 100d$ and the number of particles varied from a few hundred to 20 000. Here we present results for $N = 10\,000$, i.e., a pile roughly 100 particles deep.

We use contact force models that have similarities with those of Cundall and Strack [17] for normal forces and those of Walton and Braun [10,18] for shear (friction) forces. Static friction is implemented by keeping track of the elastic shear displacement throughout the lifetime of a contact. For two contacting particles at positions $\mathbf{r}_1$ and $\mathbf{r}_2$, with velocities $\mathbf{v}_{1,2}$ and angular velocities $\omega_{1,2}$, the force on particle 1 is computed as follows: The normal compression δ, normal velocity $\mathbf{v}_n$, relative surface velocity $\mathbf{v}_t$, and the rate of change of the elastic tangential displacement $\mathbf{u}_t$, set to 0 at the initiation of a contact, are given by

$$\delta = d - ||\mathbf{r}_{12}||, \tag{1}$$

$$\mathbf{v}_n = \mathbf{v}_{12} \cdot \hat{r}_{12}, \tag{2}$$

$$\mathbf{v}_t = \mathbf{v}_{12} - \mathbf{v}_n - (\omega_1 + \omega_2) \times \mathbf{r}_{12}/2, \tag{3}$$

$$\frac{d\mathbf{u}_t}{dt} = \mathbf{v}_t - \frac{(\mathbf{u}_t \cdot \mathbf{v}_{12})\mathbf{r}_{12}}{||\mathbf{r}_{12}||^2}, \tag{4}$$

where $\mathbf{r}_{12} = \mathbf{r}_1 - \mathbf{r}_2$, $\hat{r}_{12} = \mathbf{r}_{12}/||\mathbf{r}_{12}||$, and $\mathbf{v}_{12} = \mathbf{v}_1 - \mathbf{v}_2$. The second term in Eq.(4) arises from the rigid body rotation around the contact point and assures that $\mathbf{u}_t$ always remains in the local tangent plane of contact. Normal and tangential forces acting on particle 1 are given by

$$\mathbf{F}_n = k_n f(\delta/d)\,(\delta \hat{r}_{12} - \tau_n \mathbf{v}_n)\,, \tag{5}$$

$$\mathbf{F}_t = k_s f(\delta/d)\,(-\mathbf{u}_t - \tau_s \mathbf{v}_t)\,, \tag{6}$$

where $k_{n,s}$ and $\tau_{n,s}$ are elastic constants and viscoelastic relaxation times respectively; $f(x) = 1$ for damped linear springs or $f(x) = \sqrt{x}$ for Hertzian contacts between spheres. In addition, the magnitude of $\mathbf{u}_t$ is truncated as necessary at every time step to satisfy a local Coulomb yield criterion, $F_t < \mu F_n$. Thus, the contact surfaces are treated as "stuck" while $F_t < \mu F_n$, and slipping while the yield criterion is satisfied. This "proportional loading" approximation [19] is a simplification of the much more complicated and hysteretic behavior of real contacts [20]. The force on particle 2 is determined simply from Newton's second law, and in addition, each particle is subject to a body force

$$\mathbf{F}_{\text{body}} = mg(-\hat{z}\cos\theta + \hat{x}\sin\theta). \tag{7}$$

All results are given in terms of non-dimensionalized quantities: Distances, times, velocities, forces, elastic constants and stresses are reported in units of d, $t_0 \equiv \sqrt{d/g}$, $v_0 \equiv \sqrt{gd}$, $F_0 \equiv mg$, $k_0 \equiv mg/d$ and $\sigma_0 \equiv mg/d^2$, respectively. The summary of parameters used in the simulations are shown in Table I. For an accurate simulation of glass spheres with a diameter of $100\mu m$, the appropriate elastic constant would have had to be $k_n^{\text{glass}}/k_0 \approx 3 \times 10^{10}$, which would prohibit any reasonable large-scale simulation attempt. We use the value $k_n/k_0 = 2 \times 10^5$, assuming that the granular dynamics for this value is representative of the $k_n \to \infty$ limit of small deformations, provided that other critical parameters, such as the coefficient of restitution for binary collisions are kept constant by adjusting τ_n. Simulations for $k_n/k_0 = 2 \times 10^4$ and 2×10^6 in 2D gave essentially the same results, supporting this assumption [21].

Dimension	Force Law	k_n/k_0	τ_n/t_0	k_s/k_n	τ_s/τ_n	μ
2D	Linear	2×10^5	8.375×10^{-5}	2/7	0	0.5
3D	Hertzian	2×10^5	1.25×10^{-4}	2/7	0	0.5

TABLE I. Simulation parameters for results shown. The normal coefficient of restitution for 2D simulations is 0.92; it is a function of collision velocity for Hertzian contacts in 3D simulations.

DISCLAIMER

DISCLAIMER

Portions of this document may be illegible in electronic image products. Images are produced from the best available original document.

For Hertzian contacts, the ratio k_s/k_n depends on the Poisson Ratio of the material [20], and is about 2/3 for most materials. We use the value $k_s/k_n = 2/7$ since this makes the period of normal and shear contact oscillations equal to each other in the damped linear springs case [22]. The collisional dynamics are not very sensitive to the precise value of this ratio. The equations of motion for the translational and rotational degrees of freedom were integrated with either a third-order Gear predictor-corrector or velocity-Verlet scheme with a time step $\delta t = 1\times10^{-4}$. Care was taken to assure that we reached steady state. Typically it was necessary to run between $5-20\times 10^6\delta t$ to reach steady state, particularly when starting from a non-flowing state. All coarse grained quantities have been averaged both temporally (typically $2-8\times 10^6\delta t$) and spatially over slices of constant z.

The main characteristics of all the granular flows are: (i) The existence of an "angle of repose" θ_r, such that granular flows can not be sustained for $\theta < \theta_r$, (ii) a steady-state flow with a packing fraction independent of depth for $\theta_r < \theta < \theta_{\max}$, and (iii) for $\theta > \theta_{\max}$, development of a shear thinning layer at the bottom of the pile that results in lift-off and unstable acceleration of the entire pile. For very thin piles, less than about 20 layers, the value of θ_r depends on the depth of the pile in agreement with experiment [15]. Here we consider only deep piles where the value of θ_r is independent of depth, and focus our attention on region (ii). As seen in Fig. 1, the packing fraction ϕ remains constant as a function of depth, away from the free surface and the bottom wall. Its value is shown as a function of θ in Fig. 2. Results in 2D for systems of size 5000 and 20000 demonstrate that the thicknesses of the boundary layers at the bottom and top are independent of the height of the pile. The data suggest a tilt dependence for ϕ of the form

$$\phi_{2D}(\theta) \approx \phi_{2D}^{\max} - c_{2D}(\theta-\theta_{r,2D})^2, \quad (8)$$

$$\phi_{3D}(\theta) \approx \phi_{3D}^{\max} - c_{3D}(\theta-\theta_{r,3D}), \quad (9)$$

where $\phi_{2D}^{\max} = 0.81(1)$ and $\phi_{3D}^{\max} = 0.60(1)$. In 2D, upon lowering the tilt angle below θ_r, we observe a compaction to a polycrystalline triangular lattice with $\phi_{2D} \approx 0.9$. This causes considerable hysteresis in 2D simulations as θ is subsequently increased beyond θ_r: For the system to begin flowing, one must exceed the maximum angle of stability in order for the non-flowing state to fail. Initial failure always occurs at the bottom of the pile, followed by movement of a dilation front towards the top of the pile. Once the system has reached steady state, θ can be reduced and the system will continue to flow provided that $\theta > \theta_r$. On the other hand, in 3D there is no jump in ϕ as the pile comes to a stop. Consequently, there is no detectable hysteresis in any of the 3D simulations and the state of the pile seems to be uniquely determined by the tilt angle.

Based on runs with varying depth and width, we expect the relationship between stress and strain rate in the constant packing fraction region to be a property of the bulk. Thus, this geometry allows us to study relationships between the stress tensor and the strain rate at a given packing fraction. At a given tilt angle, two components of the stress tensor are fixed by force balance; at steady-state, the layer at depth z must carry the weight of all the spheres above it:

$$\sigma_{zz}(z) = mg\cos\theta\int_z^\infty dz\rho(z) = mg\rho\cos\theta(z_{\rm top}-z), \quad (10)$$

$$\sigma_{xz}(z) = \sigma_{zz}(z)\tan\theta, \quad (11)$$

where ρ is the number density of spheres, related to the packing fractions shown in Fig. 2 through $\phi_{2D} = \pi\rho d^2/4$ and $\phi_{3D} = \pi\rho d^3/6$. The second equality in Eq.(10) applies only to the region of constant density; $z_{\rm top}$ marks the position of an effective surface that the region of constant packing fraction sees. σ_{xx} cannot be determined from these considerations. Under conditions where the grains behave roughly like a fluid, one might expect all normal stresses, i.e., diagonal terms in the stress tensor, to be equal to each other. We observe that although $\sigma_{xx} \approx \sigma_{zz}$, there are small but systematic deviations that vary rapidly in the dilatant surface layer but become independent of depth in the region with constant packing fraction. As a measure of this anisotropy, Fig. 2 shows the tilt dependence of the normal stress anomaly in the bulk, $(\sigma_{xx}-\sigma_{zz})/\sigma_{xz}$. The origin of these deviations is not clear; they remain too small as $\theta \to \theta_r$ to be attributed to an active Rankine state [3], for which $(\sigma_{xx}-\sigma_{zz})/\sigma_{xz} = 2(\tan\theta_r)^2 \approx 0.2$. Furthermore, in all 3D runs, σ_{yy} is smaller than the other normal stresses by $10-15\%$, suggesting that consolidation and compaction normal to the shear plane is poorer. This is consistent with anisotropy observed in the static two-body correlation function [9].

Another question of particular interest is the relationship between the stress and strain rate tensors. Apart from a diagonal hydrostatic pressure term, this relationship is linear for viscous fluids and quadratic for granular systems in the Bagnold grain-inertia regime. The latter result is quite general, as it is required by dimensional analysis: In a granular system, when contact forces become large compared to the weight of individual particles but not large enough to significantly distort the spheres ($1 \ll \sigma/\sigma_0 \ll k_n/k_0$), the only relevant time scale is the inverse of the strain rate $\dot\gamma$, and the only dimensionally correct form is $\sigma \propto \dot\gamma^2$, with the ratio of the two quantities being a function of dimensionless parameters such as packing fraction and coefficient of restitution. As an example, Fig. 3 shows the relationship between shear strain rate $\partial v_x/\partial z$ and shear stress σ_{xz} for 2D and 3D cases. Below the first 6-8 layers, and away from the bottom wall, both systems exhibit Bagnold scaling, indicated by the dashed lines in Fig. 3. Data for 2D suggest an offset

of about $1.5\sigma_0$ in the stress, possibly due to corrections from the body force on individual spheres. Such an offset is not needed for an acceptable fit to the 3D data.

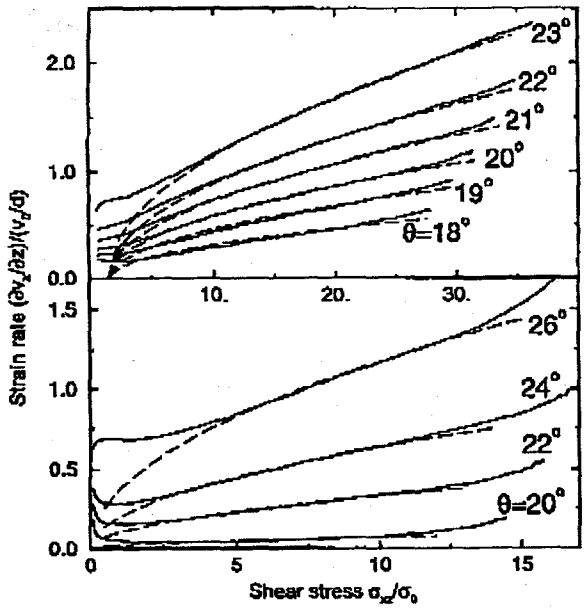

FIG. 3. Strain rates plotted as a function of shear stress σ_{xz} for 2D (top) and 3D (bottom) reveal Bagnold scaling (dashed lines) in the constant packing fraction regime away from the free surface and the bottom wall. For 2D, an offset of $1.5\sigma_0$ in the shear stress was needed for an acceptable fit. Since σ_{zz} grows linearly with depth, the figure also reflects how the strain rate varies with depth.

In order to probe the sensitivity of the results to the particular force scheme selected; we have also performed runs in the 3D system with linear damped springs, keeping all other parameters fixed [9]. Remarkably, the packing fraction profiles and the normal stress anomaly remained virtually the same, and strain rate profiles were changed only by a global factor of about 1.35. This suggests that the packing of spheres and the network of force chains they create during flow are not too sensitive to the exact form of the stiff elastic response, as long as they are subject to the same Coulomb yield criterion.

The lack of a regime with only surface flow is in rather striking contrast with experimental observations [2]. Most experiments are known to have significant side-wall effects that need to be taken into account in order to explain such surface flows [8]. Since periodic boundary conditions are used, our simulations correspond to an infinitely large box with finite depth, where the tilt angle of the free surface is fixed. In the absence of side-wall effects, the lack of surface flow can be understood as a manifestation of differing stability criteria at the surface and inside the pile (or the bottom wall.) Whereas internal failure involves significant sliding and is strongly affected by the inter-grain friction coefficient μ, surface failure is typically initiated by the *rolling* of the spheres at the surface out of their metastable traps, and is rather insensitive to μ. For small values of μ, the critical angle of stability for internal failure, $\theta_c^{\rm int}$, is smaller than the critical angle for surface stability, $\theta_c^{\rm surf}$. Stable surface flows are possible only for $\theta_c^{\rm surf} < \theta < \theta_c^{\rm int}$. Increasing μ in 3D simulations indeed results in enhanced dilational surface flow and suppressed bulk flow [9], but does not achieve surface-only flows. Although there is no fundamental reason that prohibits surface-only flows in general, it appears that contrary to prevailing wisdom, they are unlikely to occur in a pile of monodisperse spheres.

DL gratefully acknowledges support from the Israel Science Foundation under grant 211/97. Sandia is a multiprogram laboratory operated by Sandia Corporation, a Lockheed Martin Company, for the United States Department of Energy under Contract DE-AC04-94AL85000.

* E-mail address: mdertas@cerenj.com.

[1] C. A. Coulomb, Mem. de Math. de l'Acad. Royales des Science **7** 343 (1776).
[2] H. M. Jaeger, S. R. Nagel, and R. P. Behringer, Rev. Mod. Phys. **68**, 1259 (1996).
[3] R. M. Nedderman, *Statics and Kinematics of Granular Materials* (Cambridge University Press, Cambridge, England,1992).
[4] R. L. Brown and J. C. Richards, *Principles of Powder Mechanics* (Pergamon Press, Oxford, England, 1970).
[5] K. L. Johnson, *Contact Mechanics* (Cambridge University Press, New York, 1985).
[6] L. P. Kadanoff, Rev. Mod. Phys. **71**, 435 (1999).
[7] R. A. Bagnold, Proc. Roy. Soc. London A **225**, 49 (1954); *ibid.*, **295**, 219 (1966).
[8] S. B. Savage, J. Fluid Mech. **92**, 53 (1979).
[9] L. Silbert *et al.*, to be published.
[10] O. R. Walton, Mech. Mater. **16**, 239 (1993).
[11] X. M. Zheng and J. M. Hill, Powder Tech. **86**, 219 (1996).
[12] O. Pouliquen and N. Renaut, J. Phys. II France **6**, 923 (1996).
[13] T. Pöschel, J. Phys. II France **3**, 27 (1993).
[14] T. Drake, J. Geophysical Res. **95**, 8681 (1990).
[15] O. Pouliquen, Phys. Fluids **11**, 542 (1999).
[16] D. Hirshfield and D. C. Rapaport, Phys. Rev. E **56**, 2012 (1997).
[17] P. A. Cundall and O. D. L. Strack, Geotechnique **29**, 47 (1979).
[18] O. R. Walton and R. L. Braun, J. Rheol. **30**, 949 (1986).
[19] T. C. Halsey and D. Ertaş, Phys. Rev. Lett. **83**, 5007 (1999).
[20] R. D. Mindlin and H. Deresiewicz, L. Appl. Mech. **20**, 327 (1953).
[21] The $k_n \to \infty$ limit is still quite different from a hard-sphere system with only instantaneous and binary collisions, as collisions typically overlap and binary collisions are not very common except at the surface layer.
[22] J. Schäfer, S. Dippel and D. E. Wolf, J. Phys. I France **6**, 5 (1996).